An Improved Trajectory Model to Evaluate the Collection Performance of Snow Gauges

MATTEO COLLI

Department of Civil, Chemical and Environmental Engineering, University of Genoa, and WMO/CIMO Lead Centre "B. Castelli" on Precipitation Intensity, Genoa, Italy

ROY RASMUSSEN

National Center for Atmospheric Research, Boulder, Colorado*

JULIE M. THÉRIAULT

Department of Earth and Atmospheric Sciences, Université du Québec à Montréal, Montreal, Quebec, Canada

LUCA G. LANZA

Department of Civil, Chemical and Environmental Engineering, University of Genoa, and WMO/CIMO Lead Centre "B. Castelli" on Precipitation Intensity, Genoa, Italy

C. BRUCE BAKER AND JOHN KOCHENDORFER

Atmospheric Turbulence and Diffusion Division, National Oceanic and Atmospheric Administration, Oak Ridge, Tennessee

(Manuscript received 21 January 2015, in final form 1 May 2015)

ABSTRACT

Recent studies have used numerical models to estimate the collection efficiency of solid precipitation gauges when exposed to the wind in both shielded and unshielded configurations. The models used computational fluid dynamics (CFD) simulations of the airflow pattern generated by the aerodynamic response to the gauge–shield geometry. These are used as initial conditions to perform Lagrangian tracking of solid precipitation particles. Validation of the results against field observations yielded similarities in the overall behavior, but the model output only approximately reproduced the dependence of the experimental collection efficiency on wind speed. This paper presents an improved snowflake trajectory modeling scheme due to the inclusion of a dynamically determined drag coefficient. The drag coefficient was estimated using the local Reynolds number as derived from CFD simulations within a time-independent Reynolds-averaged Navier–Stokes approach. The proposed dynamic model greatly improves the consistency of results with the field observations recently obtained at the Marshall Field winter precipitation test bed in Boulder, Colorado.

1. Introduction

Despite their importance, accurate measurements of precipitation remain a challenge. Measurement errors for solid precipitation, which are often ignored for automated systems, frequently range from 20% to 70% as a result of the observed undercatch in windy conditions (Rasmussen et al. 2012). While manual solid precipitation

* The National Center for Atmospheric Research is sponsored by the National Science Foundation.

Corresponding author address: Matteo Colli, Department of Civil, Chemical and Environmental Engineering, University of Genoa, Via Montallegro 1, CAP 16145, Genoa, Italy.
E-mail: matteo.colli@unige.it

DOI: 10.1175/JAMC-D-15-0035.1

FIG. 1. An SA-shielded Geonor 600-mm gauge installed at the Marshall Field Test Site in Boulder.

measurements have been the subject of many studies (e.g., Alter 1937; Sevruk and Klemm 1989; Sevruk et al. 1991; Larson 1993; Yang et al. 1993; Goodison et al. 1998; Sugiura et al. 2003, 2006), there have been only a limited number of coordinated assessments of the accuracy, reliability, and repeatability of automatic precipitation measurements (e.g., Tumbusch 2003; Duchon 2008; Smith 2009; Rasmussen et al. 2012; Savina et al. 2012; Wolff et al. 2014).

In operational applications, windshields are commonly used to reduce the impact of wind on solid precipitation measurements. A recent survey published by the WMO (Nitu and Wong 2010) reports that 82% of operational weighing gauges used for snow measurements are equipped with a single fence windshield. The most common single fence windshield is the Alter shield (Alter 1937). Moreover, the single Alter (SA)-shielded Geonor gauge provides reference measurements within the WMO Solid Precipitation Intercomparison Experiment (SPICE; see online at http://www.wmo.int/pages/prog/www/IMOP/intercomparisons/SPICE/SPICE.html) at all sites where a double fence intercomparison reference (DFIR) shield is not available.

The aerodynamic effects of the gauge and windshield on the flow around the gauge are responsible for a significant reduction in the collection efficiency (CE) due to the deflection of particle trajectories near the gauge orifice (Goodison et al. 1998; Yang et al. 1999; Rasmussen et al. 2012; Thériault et al. 2012; Colli 2014). Snow precipitation measurements from different collocated gauge–windshield configurations in windy conditions show widely differing accumulations (Rasmussen et al. 2012). The assessment of the exposure problem for various gauge–windshield configurations is recognized as a central objective of the current Solid Precipitation Intercomparison Experiment of the WMO (Nitu et al. 2012).

The development of robust transfer functions requires a better understanding of the fundamental processes governing the wind-induced undercatch. These include the detailed wind flow patterns surrounding the gauge–windshield configuration and the snowflake trajectories, which in turn depend on the snowflake microphysical characteristics (snow crystal type, fall speed, and size distribution). The goal of this modeling work is to better understand the mean collection efficiency and its variability at any given wind speed, building upon the studies of Thériault et al. (2012) and Colli (2014). To address this, high-space- and high-time-resolution computational fluid dynamics (CFD) was used to simulate the flow past an SA-shielded (Fig. 1) and an unshielded Geonor 600-mm gauge.

A trajectory model initialized with the flow field was used to compute the collection efficiency. The main advantage of studying the collection efficiency by means of CFD numerical models is the possibility to isolate the exposure effect from the other sources of uncertainty occurring in the field. The results were compared with catch efficiency measurements from the Marshall Field winter precipitation test bed in Boulder, Colorado.

2. Field observations

The CE is typically calculated by comparing the snow accumulation P over a set time period (typically 30–60 min)

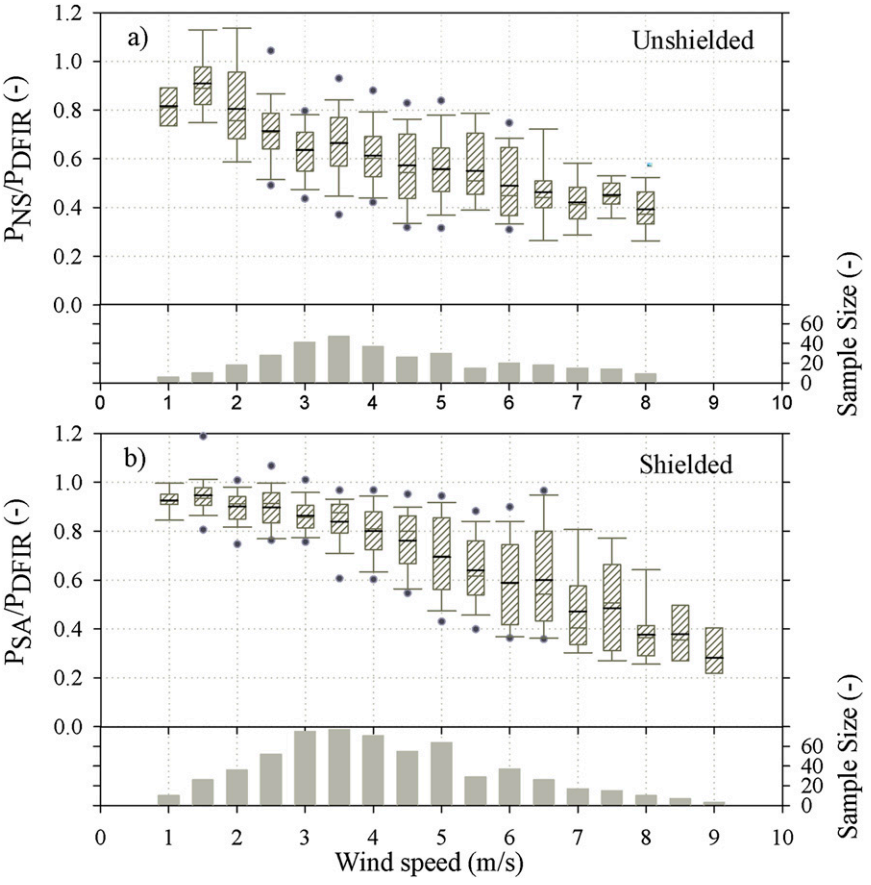

FIG. 2. Collection efficiency computed as the ratio between precipitation measurements from an (a) unshielded and (b) SA-shielded gauge against a DFIR-shielded gauge with varying wind speed. The data are sampled with a 30-min period and averaged over 0.5 m s^{-1} wind speeds bins. Boxes enclose data within the 25th and 75th percentiles while whiskers are for the 10th and 90th percentiles and dots are for the 5th and 95th percentiles. Lines within each box indicate the mean (thick) and the median (thin) values. Data are for snow conditions as identified by a Present Weather Detector (Vaisala PWD22) from 2009 to 2013 at the Marshall Field Test Site.

for a given gauge–windshield configuration with a reference accumulated snow measurement. The DFIR is often used as the reference, since it is the WMO reference snow measurement system (Goodison et al. 1998). Because of the complex interaction among the airflow, the snowflakes, and the various gauge–windshield systems, large unexplained uncertainties exist in the derivation of the transfer functions. The temporal and spatial variability of the wind and precipitation near the gauge and windshield, unsteady flow patterns generated by the windshields themselves, and the variability of snowflake type, terminal velocity, and size distribution lead to a variety of possible trajectories past the gauge for a given wind field (e.g., Rasmussen et al. 2012; Thériault et al. 2012).

Figure 2a shows the ratio of snow precipitation measurements from a 2-m-high unshielded Geonor T200B P_{NS} and a 3-m-high DFIR-shielded Geonor T200Bs P_{DFIR} as a function of wind speed from data collected at the Marshall Field Test Site between 2009 and 2013. The data are binned over 0.5 m s^{-1} wind speed intervals measured at the 2-m level. Only 30-min data pairs in which the DFIR Geonor accumulation is larger than 0.25 mm are included to eliminate spurious ratios from being included as a result of small errors when both values are small. The snowfall amounts were sampled over a 30-min time period in order to reduce the effects of the time variability of the precipitation and the wind speed. Accumulation amounts at time periods less than 30 min do not provide a reliable precipitation amount owing to the limited ability of the Geonor gauge to measure smaller than 0.25 mm. Further information about the test bed and the installed instrumentation are provided by Rasmussen et al. (2012).

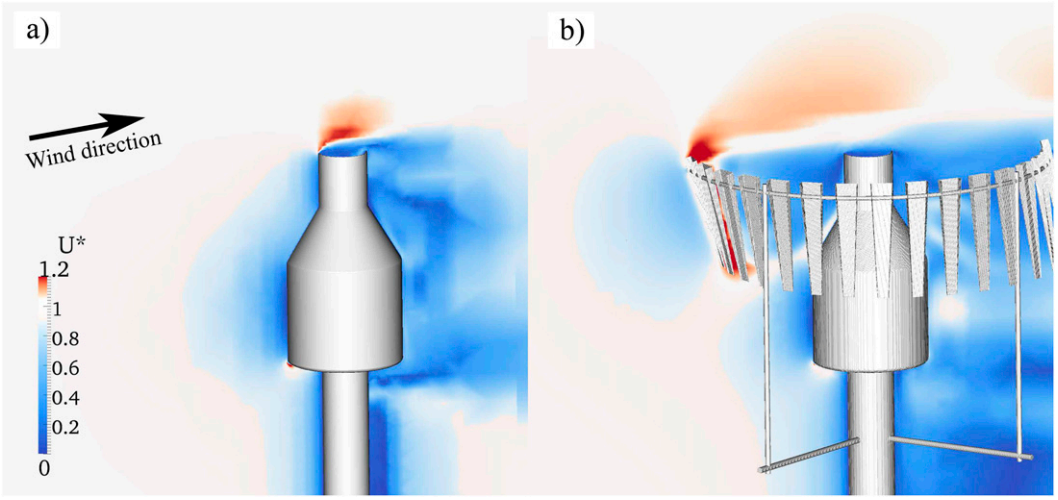

FIG. 3. Nondimensional magnitude of velocity (unitless) color plots for an (a) unshielded and (b) SA-shielded Geonor 600-mm gauge. The airflow has been simulated by using a RANS k–Ω SST model.

A noticeable wind-induced underestimate of the precipitation accumulation is shown in Fig. 2a by the mean P_{NS}/P_{DFIR} ratio (thick lines inside the box plots), which quickly decreases as the wind speed increases from 1 to 6 m s^{-1} and tends to an asymptotic value of 0.4 beyond 6 m s^{-1}. In addition to the reduction of the catch ratio with increasing wind speed, the box plots show a wide scatter for a given wind speed. This makes the application of a unified transfer function challenging.

Similarly, Fig. 2b presents snow measurements obtained from a 2-m-high SA-shielded Geonor T200B P_{SA}. In this case, the mean P_{SA}/P_{DFIR} ratios show a slower decrease with respect to the unshielded case with higher values of the catch ratio initially, approaching a value of 0.4 beyond 6 m s^{-1}.

The comparison between P_{NS}/P_{DFIR} and P_{SA}/P_{DFIR} reveals that a characteristic of both curves is the large scatter for a given wind speed.

3. The airflow and trajectory model

Following Nešpor and Sevruk (1999), a CFD finite volume method has been successfully adopted to solve the three-dimensional equations for the airflow around the SA-shielded and unshielded Geonor T200B gauge systems. The spatial domain has been subdivided in 7.5×10^6 (unshielded geometry) and 10.0×10^6 (shielded geometry) hexahedral cells with different degrees of refinements near to the gauge–windshield surfaces in order to reach numerical convergence. The time-averaged air velocity, turbulent kinetic energy, and pressure fields have been solved by means of a Reynolds-averaged Navier–Stokes (RANS) turbulent kinetic energy–specific dissipation (k–Ω) SST model (Colli 2014; Colli et al. 2015a, manuscript submitted to *J. Hydrometeor.*).

Figure 3 presents color plots of the nondimensional magnitude of velocity U^* (unitless) for a streamwise vertical section passing through the center of the gauge for the unshielded (Fig. 3a) and SA-shielded (Fig. 3b) gauge. The U^* values have been obtained by normalizing the local magnitude of velocity value with the undisturbed wind speed U_w (m s^{-1}). A comparison between the two airflows confirms the advantage of using a single Alter shield to reduce the velocity magnitude in the region contained within the fence and hence the exposure of the gauge to the wind. The trajectories of dry and wet snow particles as defined by Rasmussen et al. (1999) were computed for wind speeds between 1 and 10 m s^{-1} by means of a Lagrangian scheme applied to the time-averaged airflows.

Figure 4 shows the precipitation trajectories and the airflow vectors computed for sample unshielded (Fig. 4a) and SA-shielded (Fig. 4b) cases with the horizontal U_w equal to 4 m s^{-1} and dry snow particles with diameter d_p equal to 5 mm. The strong updrafts observed immediately upwind the unshielded collector cause an upward deflection of the trajectories with a consequent reduction of the number of collected particles.

A different situation is observed for the SA-shielded gauge as shown in Fig. 4b. The deformation of the airflow due to the aerodynamic response of the upwindshield elements and the consequent shift of the particle trajectories before the gauge collector are evident. However, a reduction of the airflow vertical components u_z (m s^{-1}) near the collector results in a larger

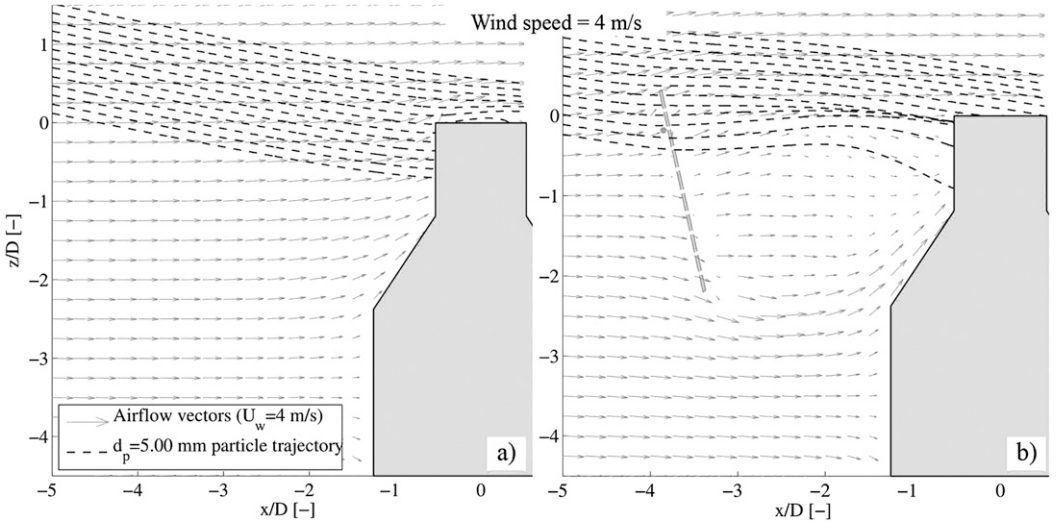

FIG. 4. (a) Unshielded and (b) SA-shielded Geonor 600-mm gauge, showing a sample dry snow (d_p = 5 mm) particle trajectories plot (black lines) and vector plot (gray lines) on a vertical plane as computed by the RANS airflow and the Lagrangian tracking model at a horizontal wind speed equal to 4 m s^{-1}. The spatial coordinates x and z are normalized with the gauge collector diameter D.

number of collected particles with respect to the unshielded case. Figure 5 details the magnitude of the air vertical velocity near the gauge and the upwind single Alter elements. It is shown that a horizontal $U_w = 4\,\mathrm{m\,s^{-1}}$ causes an updraft bigger than $1\,\mathrm{m\,s^{-1}}$ near the collector with an immediate impact on the trajectories (Fig. 5a). When the single Alter shield is included in the simulations (Fig. 5b) the vertical air velocity contours do not reveal significant values near the gauge collector ($u_z \approx 0\,\mathrm{m\,s^{-1}}$). In this case, the deformation of the particle trajectories is mainly due to the influence of the up-windshield elements on the air magnitude of the U^* field that is mainly influenced by the horizontal components (red zones in Fig. 3). The formation of trajectories clusters and divergence zone has been detailed by Colli et al. (2015b, manuscript submitted to *J. Hydrometeor.*).

The influence of the single Alter windshield on the collection efficiency of the gauge can be quantified using an inverse exponential size distribution (Marshall and Palmer

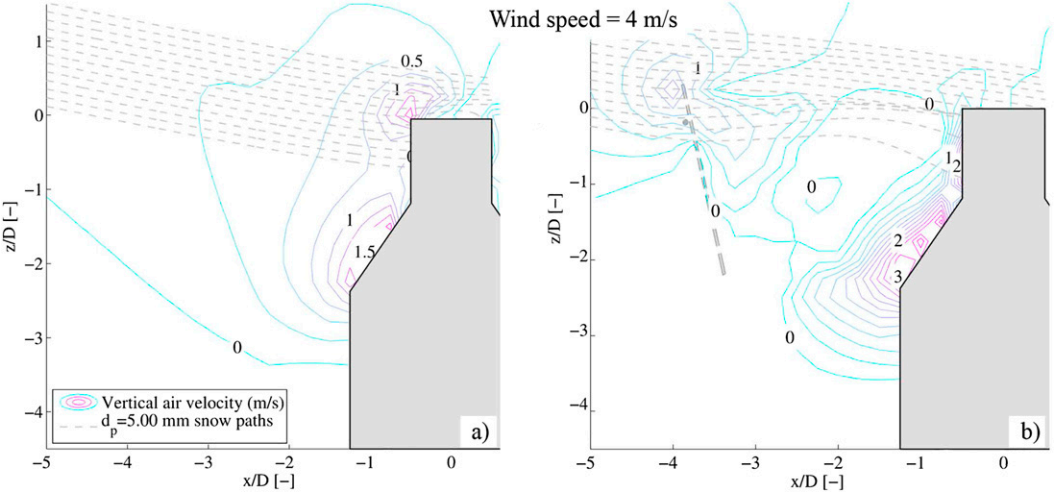

FIG. 5. (a) Unshielded and (b) SA-shielded Geonor 600-mm gauge, showing a sample dry snow (d_p = 5 mm) particle trajectories plot (gray lines) and vertical air velocity (m s^{-1}) contour plot (colored lines) on a vertical plane as computed by the RANS airflow and the Lagrangian tracking model at a horizontal wind speed equal to 4 m s^{-1}. The spatial coordinates x and z are normalized with the gauge collector diameter D, and the representation plane passes through the open space between two SA shield elements.

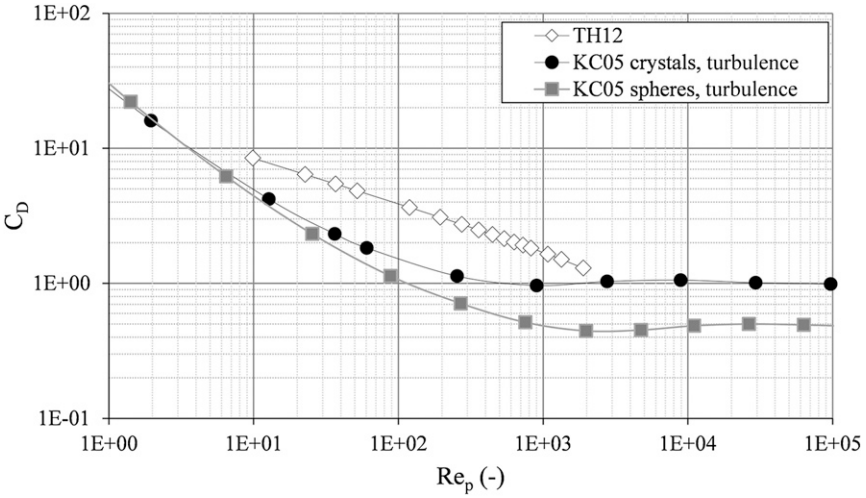

FIG. 6. Drag coefficient (unitless) vs particle Reynolds numbers (unitless) for spheres and crystals based on Khvorostyanov and Curry (2005) (black circles and gray squares, respectively) in comparison with the Thériault et al. (2012) formulation (open diamonds).

1948) and counting the precipitation volume associated with the collected particles (Thériault et al. 2012; Colli et al. 2015b, manuscript submitted to *J. Hydrometeor.*). The particle size distribution was calculated as follows:

$$N(d_p) = N_0 e^{-\lambda d_p}, \tag{1}$$

where reference values for the intercept parameter $N_0 = 5 \times 10^6\,\mathrm{m}^{-4}$ and the slope parameter $\lambda = 0.50\,\mathrm{mm}^{-1}$ were assumed according to Thériault et al. (2012).

The Lagrangian trajectories model (LTM) adopted in previous studies (Nešpor and Sevruk 1999; Thériault et al. 2012; Colli 2014) solves the equations of the particles motion by assuming constant values of the drag coefficient C_D along the particle trajectory [Eq. (2)]. The drag coefficient is calculated from the particle terminal velocity w_T derived from the mass-dimensional relationships presented in Rasmussen et al. (1999):

$$C_D = \frac{2V_p(\rho_p - \rho_a)g}{A_p \rho_a w_T^2}, \tag{2}$$

where g is the gravity acceleration, V_p is the particle volume, A_p is the cross-sectional area, and ρ_a (ρ_p) is the density of the air (snow particle). Previous estimates of collection efficiency using CFD modeling tended to underestimate the actual values (Thériault et al. 2012). In this study, improvements to the drag coefficient proposed by Beard (1980) and Böhm (1992) are evaluated. They expressed the relationship between C_D and the particle Reynolds number Re_p in terms of the nondimensional Best number $X = C_D \mathrm{Re}_p^2$. A comparative analysis of various studies conducted by Mitchell (1996) suggested a power-law relation for $\mathrm{Re}_p(X) = a_{\mathrm{Re}} X^{b_{\mathrm{Re}}}$, with numerical fits for the coefficients a_{Re} and b_{Re} computed for different types of precipitation. The effect of turbulence in the flow induces a slight increase of the drag coefficient with respect to the above formulation around $\mathrm{Re}_p \approx 10^3$ (Khvorostyanov and Curry 2005). The transition regime between laminar and turbulent flow was studied by Böhm (1992), which related the turbulent drag coefficient C_{D_t} to the laminar drag coefficient C_{D_l} using an interpolation function.

Khvorostyanov and Curry (2005) corrected the parameterization of Mitchell to deduce power-law coefficients a_{Re_t} and b_{Re_t} as continuous analytical functions of the Best (or Reynolds) number and of the particle size in a turbulent flow for spherical and crystal particles. They also performed an in-depth analysis of the asymptotic values of a_{Re_t} and b_{Re_t} and corrections for temperature and pressure. This formulation accurately reproduced the observed terminal velocity of a wide range of particle sizes and densities. The formulation by Khvorostyanov and Curry (2005) had lower values of C_D (Fig. 6), leading to a higher terminal velocity and higher collection efficiency relative to Thériault et al. (2012), which used a higher drag coefficient.

Three different versions of the LTM have been prepared to test the effect of various C_D formulations on the gauge collection efficiency (Fig. 6). The first one used the approach from Thériault et al. (2012) and Colli (2014) assuming fixed C_D values along the particle

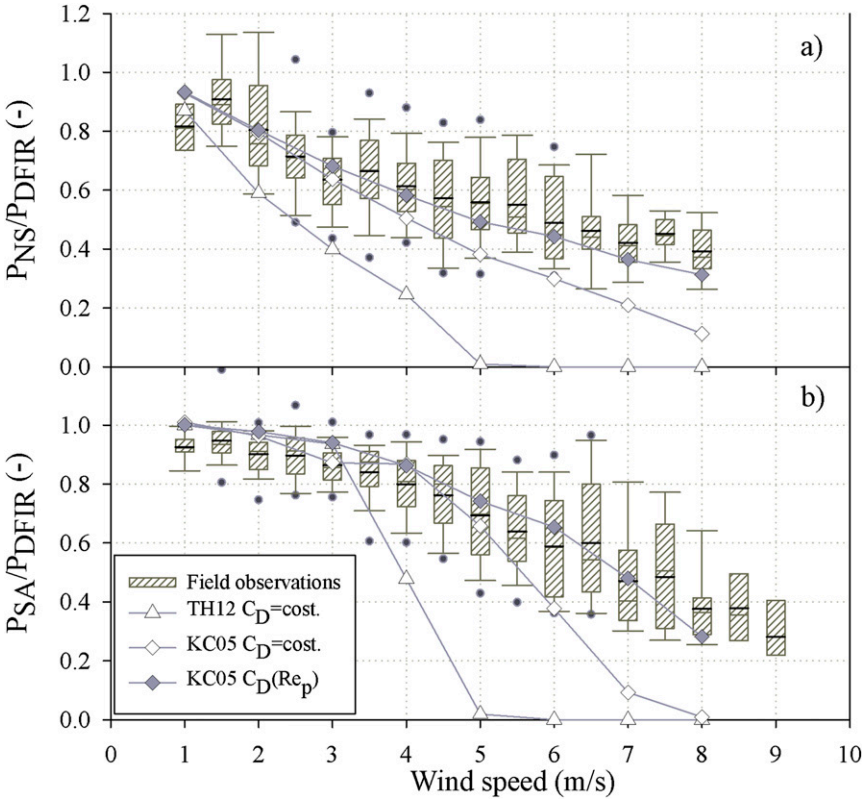

FIG. 7. Collection efficiency (unitless) vs horizontal wind speed (m s^{-1}) for dry snow ($N_0 = 5 \times 10^6$ m^{-4} and $\lambda = 0.50$ mm^{-1}) particles computed by the CFD RANS methodology and the LTM for an (a) unshielded and (b) SA-shielded Geonor 600-mm gauge. The constant drag coefficient formulation (TH12) by Thériault et al. (2012) (open triangles), and the Khvorostyanov and Curry (2005) drag coefficient formulation (KC05) using the particle terminal velocity to calculate the applied C_D along a time-varying trajectory (open diamonds), and calculating the C_D based on the particle-to-air velocity (gray diamonds) are compared. The Marshall Field Test Site data are shown in the background.

trajectory [Eq. (2)] and therefore constant terminal velocities. The second method employed the Khvorostyanov and Curry (2005) curves for crystal particles in turbulent flow (Fig. 6) to compute the drag coefficient while still assuming a constant value of C_D along the particle trajectory. The third approach removed this assumption by dynamically updating the crystals drag coefficient in turbulent flow according to Re_p and hence the particle-to-air velocity $|\mathbf{v}_p\mathbf{v}_a|$, where $\mathbf{v}_p$ and $\mathbf{v}_a$ are the particle and the air velocity vectors, respectively.

4. Collection efficiency results

Figures 7a and 7b compare the collection efficiency results obtained from the LTM employing the constant drag coefficient formulation used in Thériault et al. (2012) and those obtained with the new approach for dry snow falling near an SA-shielded and an unshielded Geonor gauge. Some deviations between LTM results and field observations are expected given the different nature of the reference amount of precipitation adopted by the two approaches to derive CE. If the observations from the field assume the DFIR measurements as the best estimate of the true precipitation (unknown), the LTM relies on known values of a synthetic accumulated precipitation. An in-depth analysis of the DFIR collection performance for solid precipitation is provided by Thériault et al. (2015).

This notwithstanding, the two new models based on the Khvorostyanov and Curry (2005) drag coefficient formulation provide a better comparison to the observations. The first model estimated the drag coefficient assuming a spherical shape, using the particle terminal velocity to calculate the Reynolds number as shown in Fig. 6, leading to lower collection efficiencies than those observed in the field, as shown in Figs. 7a and 7b. The

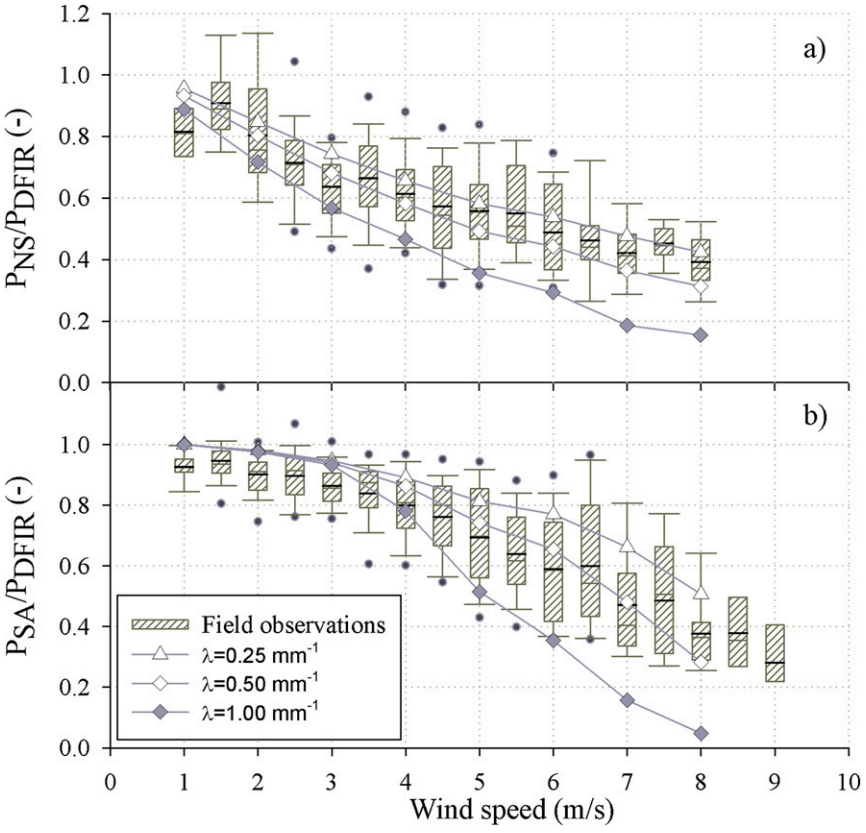

FIG. 8. Collection efficiency (unitless) vs horizontal wind speed (m s^{-1}) for an (a) unshielded and (b) SA-shielded Geonor 600-mm gauge computed by the snowflake trajectory model (C_D from KC05) based on the RANS time-averaged flow field. Three different particle size distributions for snow are simulated according to the slope parameter (mm^{-1}). The Marshall unshielded gauge data are shown in the background.

adoption of the Khvorostyanov and Curry (2005) C_D formulation brings the modeled collection efficiencies close to the lower bounds of the field data (open diamonds). When the particle-to-air velocity is also incorporated in the Reynolds number and the associated drag coefficient calculations (gray diamonds) the collection efficiency increases even further, which agrees well with the observations. The reason for this behavior can be diagnosed from Fig. 6. Since the drag coefficient decreases with increasing Reynolds number, increased wind velocities result in lower drag coefficients and higher terminal velocities and, therefore, higher collection efficiencies.

Figure 8a presents a comparison of the simulated collection efficiency for an unshielded gauge for three different snow particle size distributions based on field observations by Houze et al. (1979) and Thériault et al. (2012) using the dynamically updated Khvorostyanov and Curry (2005) drag coefficient formulation.

The simulated collection efficiency spans the range of the observational data, confirming the suggestion by Thériault et al. (2012) that the variability in snow particle size distribution may be one of the primary causes for the observed scatter in the collection efficiency observed in this and other data. At higher wind speeds, the scatter of the observed data is highly variable and in general narrower than the simulation results. This may be due to the limited sample of unshielded gauge measurements obtained under severe wind regimes. Figure 2 shows that when $U_w > 6\,\mathrm{m\,s^{-1}}$, the sample size of each bin varies between 9 and 18 events. A similar plot for a single Alter gauge (Fig. 8b) shows good agreement with the data throughout the wind speed range. It is apparent from the plot that the single Alter shield increases the gauge collection efficiency at intermediate wind speeds (3–6 m s^{-1}) but may actually have a lower collection efficiency than an unshielded gauge at wind speeds greater than 7 m s^{-1}. The variability in the data is nicely explained by the variation in size distribution, with the steeper distribution ($\lambda = 1.00\,\mathrm{mm^{-1}}$) having the smallest particles and, therefore, lower terminal velocity and lower collection efficiency, while the size distribution

TABLE 1. Sigmoid fit parameters a, b, c, and d of the collection efficiency results for different values of λ.

	P_{NS}				P_{SA}			
λ (mm^{-1})	a	b	c	d	a	b	c	d
0.25	0.28	1.72	3.67	−0.63	−0.34	1.37	2.37	9.17
0.50	0.2	1.36	2.82	1.35	−1.35	2.43	2.52	9.8
1.00	0.03	1.67	2.77	1.11	−0.02	1.05	1.1	5.21

with a shallow slope has the largest particles and the highest terminal velocity and collection efficiency. This is comparable to the results found in Thériault et al. (2012).

Wolff et al. (2014) found nonlinear mathematical relationships between collection efficiency and wind speed based on dry snow, mixed precipitation, and rain measurements made at the Haukeliseter (Norway) field site. In this work, a sigmoid law has been adopted to fit the simulated CE values for different particle size distributions in the following form:

$$f(U_w) = a + \frac{b}{[1 + e^{(U_w - d)/c}]}, \tag{3}$$

where a, b, c, and d are the regression parameters defined in Table 1. The proposed parameter combinations show a very good agreement between the regression curves and data with values of the coefficient of determination R^2 that are always greater than 0.99.

Theoretically, Fig. 8b shows that the modeled collection efficiency is independent of the size distribution up to 3 m s^{-1}. Notice that for a wind speed of 5 m s^{-1}, the effects of the different modeled size distributions explained more than 50% of the variability in the measured collection efficiency. To explore this result, observations of the snow particle size distribution measured by a disdrometer at the Marshall Field Test Site during the winters of 2003–07 were analyzed. A detailed description of the dataset is given in Brandes et al. (2007). Only the precipitation rates of 1 mm h^{-1} measured by the DFIR were used for this analysis in order to reduce the number of factors impacting the size distribution. The median diameter D_m of each size distribution averaged over 30 min have been sorted by wind speeds of 1, 2, 3, 4, and 5 m s^{-1}. The median diameter as a function of collection has been analyzed for each wind speed.

The slope of the linear relationship between the median volume diameter and the collection efficiency for a given wind speed is shown in Fig. 9. These results show that there is very little variation of the collection with the median volume diameter at wind speeds less than 3 m s^{-1} (the slope is ~0). As the wind speed increases,

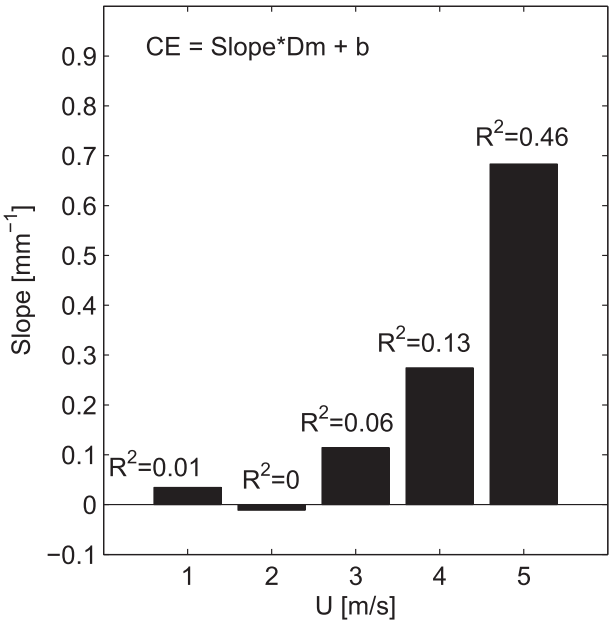

FIG. 9. Slope of the collection efficiency with the median volume diameter as a function of wind speed. The median volume diameter was measured by a disdrometer placed in a double fence similar to the DFIR. The data were collected during the winters of 2003–07 (Brandes et al. 2007) and averaged over 30 min. Only precipitation rates of 1 mm h^{-1} were used. To consider solid precipitation only, the data associated with temperatures <0°C were used.

the correlation coefficient increases starting at 3 m s^{-1}, with a sharp increase in the value of the slope between 4 and 5 m s^{-1}. As in Fig. 8b, the size distribution of snow had a negligible impact on the collection efficiency for wind speeds up to 4 m s^{-1}, which suggests that the snow particle size distribution mainly impacts the collection efficiency at wind speeds ≥5 m s^{-1}. This steep increase in collection efficiency with mean diameter at 5 m s^{-1} indicates that the size distribution associated with larger snowflakes will fall in the gauge. Many other sources of uncertainty are probably affecting the results but the observed correlation between the particle median diameter and the associated collection efficiency fits well with the theoretical CE.

5. Conclusions

The proposed dynamic formulation of the drag coefficient yielded significantly improved numerical model estimates of unshielded and single Alter–shielded Geonor snow collection efficiencies over previous formulations that relied upon a constant drag coefficient within the LTM. The drag coefficient decreases by approximately a factor of 4 using the dynamical formulation as compared with the constant drag coefficient formulation. As a result, the terminal velocity increased

by a factor of 2, leading to a higher collection efficiency, which compared well to observations of collection efficiency from the Marshall Field Test Site.

Using three different typical particle size distributions provided good agreement for a large portion of the observed catch efficiency variability. As expected, the size distribution with the larger particles had the higher collection efficiency. At low wind speeds, the updrafts induced by the gauge are relatively low in comparison with snow particle velocity, resulting in a relatively small change of collection efficiency with size distribution. As the upstream wind speed increases to $5\,m\,s^{-1}$, the updraft over the gauge becomes similar to the fall velocity of the snow particles, leading to a strong sensitivity to the particle size distribution, in agreement with observed trends at the Marshall Field Test Site.

These results show the value of using CFD and trajectory modeling to help explain the collection efficiency of snow gauges and potentially to reconstruct the actual snowfall given information about the snow particle size distribution and the snow gauge accumulation as a function of wind speed.

Numerical modeling can be used to better understand the fundamentals of the wind-induced errors of solid precipitation measurements. The current results compared well with the observations and provide insight into the physics describing the enhanced collection efficiency of a single Alter gauge system over an unshielded system.

A few limitations of the current work should be noted. First, the present work assumed uniform and steady air velocity profiles upstream of the gauge. The role of boundary layer turbulence on CE is currently being analyzed by means of more accurate time-dependent models, such as large-eddy simulation, and will be presented in Colli et al. (2015b, manuscript submitted to *J. Hydrometeor.*). The drag coefficient dynamic formulation will also be applied to the time-dependent airflows to account for the turbulence generated by oscillating single Alter shield elements. Last, more realistic hydrodynamic schemes for the computation of hydrometeor trajectories and the adjustment of the drag coefficient scheme for nonspherical particles should be considered.

Acknowledgments. This research was supported through funding from NOAA, NSF, the University of Genoa, and the Natural Sciences and Engineering Research Council of Canada (NSERC).

REFERENCES

Alter, J., 1937: Shielded storage precipitation gages. *Mon. Wea. Rev.,* **65,** 262–265, doi:10.1175/1520-0493(1937)65<262:SSPG>2.0.CO;2.

Beard, K., 1980: The effect of altitude and electrical force on the terminal velocity of hydrometeors. *J. Atmos. Sci.,* **37,** 1363–1374, doi:10.1175/1520-0469(1980)037<1363:TEOAAE>2.0.CO;2.

Böhm, J., 1992: A general hydrodynamic theory for mixed-phase microphysics. Part I: Drag and fall speeds of hydrometeors. *Atmos. Res.,* **27,** 253–274, doi:10.1016/0169-8095(92)90035-9.

Brandes, E. A., K. Ikeda, G. Zhang, M. Schnhuber, and R. M. Rasmussen, 2007: A statistical and physical description of hydrometeor distributions in Colorado snowstorms using a video disdrometer. *J. Appl. Meteor. Climatol.,* **46,** 634–650, doi:10.1175/JAM2489.1.

Colli, M., 2014: Assessing the accuracy of precipitation gauges: A CFD approach to model wind induced errors. Ph.D. thesis, University of Genoa, 209 pp., doi:10.13140/RG.2.1.4408.1767.

Duchon, C., 2008: Using vibrating-wire technology for precipitation measurements. *Precipitation: Advances in Measurement, Estimation and Prediction,* S. C. Michaelides, Ed., Springer, 33–58.

Goodison, B., P. Louie, and D. Yang, 1998: WMO solid precipitation measurement intercomparison: Final report. WMO Tech. Doc. 872, 212 pp. [Available online at http://library.wmo.int/opac/index.php?lvl=notice_display&id=6441#.VbiFwPntlBd.]

Houze, R. A., P. V. Hobbs, P. H. Herzegh, and D. B. Parsons, 1979: Size distributions of precipitation particles in frontal clouds. *J. Atmos. Sci.,* **36,** 156162, doi:10.1175/1520-0469(1979)036<0156:SDOPPI>2.0.CO;2.

Khvorostyanov, V., and J. Curry, 2005: Fall velocities of hydrometeors in the atmosphere: Refinements to a continuous analytical power law. *J. Atmos. Sci.,* **62,** 4343–4357, doi:10.1175/JAS3622.1.

Larson, L. W., 1993: ASOS heated tipping bucket precipitation gage (Friez) evaluation at WSFO, Bismarck, North Dakota, March 1992–March 1993. NWS Central Region Final Rep., 54 pp.

Marshall, J. S., and W. M. K. Palmer, 1948: The distribution of raindrops with size. *J. Meteor.,* **5,** 165–166, doi:10.1175/1520-0469(1948)005<0165:TDORWS>2.0.CO;2.

Mitchell, D., 1996: Use of mass- and area-dimensional power laws for determining precipitation particle terminal velocities. *J. Atmos. Sci.,* **53,** 1710–1723, doi:10.1175/1520-0469(1996)053<1710:UOMAAD>2.0.CO;2.

Nešpor, V., and B. Sevruk, 1999: Estimation of wind-induced error of rainfall gauge measurements using a numerical simulation. *J. Atmos. Oceanic Technol.,* **16,** 450–464, doi:10.1175/1520-0426(1999)016<0450:EOWIEO>2.0.CO;2.

Nitu, R., and K. Wong, 2010: CIMO survey on national summaries of methods and instruments for solid precipitation measurements at automatic weather stations. WMO Instruments and Observing Methods Tech. Rep. 102, WMO/TD 1544, 57 pp. [Available online at http://www.wmo.int/pages/prog/www/IMOP/publications/IOM-102_SolidPrecip.pdf.]

——, and Coauthors, 2012: WMO intercomparison of instruments and methods for the measurement of solid precipitation and snow on the ground: Organization of the experiment. *Extended Abstracts, WMO Technical Conf. on Meteorological and Environmental Instruments and Methods of Observations,* Brussels, Belgium, World Meteorological Organization, 10 pp. [Available online at https://www.wmo.int/pages/prog/www/IMOP/publications/IOM-109_TECO-2012/Session1/O1_01_Nitu_SPICE.pdf.]

Rasmussen, R., J. Vivekanandan, J. Cole, B. Myers, and C. Masters, 1999: The estimation of snowfall rate using visibility. *J. Appl. Meteor.,* **38,** 1542–1563, doi:10.1175/1520-0450(1999)038<1542:TEOSRU>2.0.CO;2.

——, and Coauthors, 2012: How well are we measuring snow: The NOAA/FAA/NCAR winter precipitation test bed. *Bull. Amer. Meteor. Soc.,* **93,** 811–829, doi:10.1175/BAMS-D-11-00052.1.

Savina, M., B. Schppi, P. Molnar, P. Burlando, and B. Sevruk, 2012: Comparison of a tipping-bucket and electronic weighing precipitation gage for snowfall. *Atmos. Res.,* **103,** 45–51, doi:10.1016/j.atmosres.2011.06.010.

Sevruk, B., and S. Klemm, 1989: Catalogue of national standard precipitation gauges. WMO Instruments and Observing Methods Rep. 39, WMO/TD 313, 50 pp. [Available online at https://www.wmo.int/pages/prog/www/IMOP/publications/IOM-39.pdf.]

——, J. A. Hertig, and R. Spiess, 1991: The effect of a precipitation gauge orifice rim on the wind field deformation as investigated in a wind tunnel. *Atmos. Environ.,* **25,** 1173–1179, doi:10.1016/0960-1686(91)90228-Y.

Smith, C., 2009: The relationship between snowfall catch efficiency and wind speed for the GeonorT-200B precipitation gauge utilizing various wind shield configurations. *Proc. 77th Western Snow Conf.,* Canmore, AB, Canada, 115–121.

Sugiura, K., D. Yang, and T. Ohata, 2003: Systematic error aspects of gauge-measured solid precipitation in the Arctic, Barrow, Alaska. *Geophys. Res. Lett.,* **30,** 1192, doi:10.1029/2002GL015547.

——, T. Ohata, and D. Yang, 2006: Catch characteristics of precipitation gauges in high-latitude regions with high winds. *J. Hydrometeor.,* **7,** 984–994, doi:10.1175/JHM542.1.

Thériault, J. M., R. Rasmussen, K. Ikeda, and S. Landolt, 2012: Dependence of snow gauge collection efficiency on snowflake characteristics. *J. Appl. Meteor. Climatol.,* **51,** 745–762, doi:10.1175/JAMC-D-11-0116.1.

——, ——, E. Petro, J. Trépanier, M. Colli, and L. G. Lanza, 2015: Impact of wind direction, wind speed, and particle characteristics on the collection efficiency of the double fence intercomparison reference. *J. Appl. Meteor. Climatol.,* doi:10.1175/JAMC-D-15-0034.1, in press.

Tumbusch, M., 2003: Evaluation of OTT PLUVIO Precipitation Gage versus Belfort Universal Precipitation Gage 5-780 for the National Atmospheric Deposition Program. U.S. Geological Survey Water-Resources Investigations Rep. 03-4167, 25 pp. [Available online at http://pubs.usgs.gov/wri/wrir034167/wrir034167.pdf.]

Wolff, M., K. Isaksen, A. Petersen-Øverleir, K. Ødemark, T. Reitan, and R. Bækkan, 2014: Derivation of a new continuous adjustment function for correcting wind-induced loss of solid precipitation: Results of a Norwegian field study. *Hydrol. Earth Syst. Sci. Discuss,* **11,** 10 043–10 084, doi:10.5194/hessd-11-10043-2014.

Yang, D., J. R. Metcalfe, B. E. Goodison, and E. Mekis, 1993: An evaluation of the double fence intercomparison reference gauge. *Proc. 50th Meeting of the Eastern Snow Conf.,* Quebec City, QC, Canada, 105–111.

——, and Coauthors, 1999: Quantification of precipitation measurement discontinuity induced by wind shields on national gauges. *Water Resour. Res.,* **35,** 491–508, doi:10.1029/1998WR900042.